Title: Structural relaxation and crystallisation in Fe-Cr-Si-B and Fe-Cu-Cr-Si-B amorphous alloys

Author: Zbigniew Stokłosa, Józef Rasek, Piotr Kwapuliński, Grzegorz Haneczok, Lucjan Pająk

Proceedings of the IV ISSPMS'01, Jaszowiec 2001

Structural Relaxation and Crystallisation in Fe–Cr–Si–B and Fe–Cu–Cr–Si–B Amorphous Alloys

Z. Stokłosa, J. Rasek, P. Kwapuliński, G. Haneczok and L. Pająk

Institute of Physics and Chemistry of Metals, University of Silesia
Bankowa 12, 40-007 Katowice, Poland

Structural relaxation, crystallisation and optimisation processes in soft magnetic amorphous alloys based on iron are examined by applying different experimental techniques: X-ray diffraction analysis, high-resolution electron microscopy, measurements of magnetic and electric properties (permeability, after-effect, resistivity). The presented results are discussed in terms of annealing out of microvoids, formation of a nanocrystalline phase and changes of effective magnetostriction constant.

PACS numbers: 75.50.–y, 75.75.+a

1. Introduction

In the last ten years a considerable progress in the domain of new soft magnetic materials has been observed. Amorphous alloys based on iron obtained by rapid cooling from liquid phase are one of the most interesting groups of these materials [1–6]. The main goal of this examinations is to obtain magnetic material with relatively high value of magnetic permeability and magnetic losses as low as possible. Obviously an economic aspect is also important and a good soft magnetic material cannot be very expensive. It seems all these requirements are well fulfilled for the Fe–X–Si–B group of alloys. At present it is one of the most widely studied group of amorphous and nanocrystalline alloys [6–9]. A proper chemical composition of the alloy and a suitable thermal annealing allow obtaining material very interesting for practical applications. Apart from that the problem of studying the influence of alloying additions X is still open in literature [1–3]. In the present paper we concentrate on magnetic properties of the alloys of type Fe–Cr–Si–B and Fe–Cu–Cr–Si–B.

2. Material and experimental procedure

The experiments were carried out on two groups of amorphous alloys based on iron — $Fe_{78}Si_8B_{14}$, $Fe_{76}Cr_2Si_8B_{14}$, $Fe_{74}Cr_4Si_8B_{14}$ and $Fe_{78}Si_{13}B_9$, $Fe_{75}Cu_1Cr_2Si_{13}B_9$, $Fe_{74}Cu_1Cr_3Si_{13}B_9$, $Fe_{74}Cu_1Cr_2Zr_1Si_{13}B_9$. All these alloys were obtained by melt spinning technique in the form of ribbons with thickness of about 25 μm.

The X-ray examination (Philips difractometer) and electron microscope (JEM-200B and high-resolution JEM-3010) observation confirm that in the "as quenched" state all the alloys were in amorphous state. In order to study structural relaxation and crystallisation processes two experimental techniques were used — measurements of magnetic properties (magnetic permeability, coercive field, magnetic after-effect) and electric properties (electrical resistivity and Hall constant). The experiments were carried out on samples in the "as quenched" state by applying linear heating with the rate ranging from 0.5 to 10 K/min. The Curie temperature of the examined alloys was determined from temperature dependence of magnetic permeability (heating rate — 10 K/min).

In the next step amorphous samples were annealed for one hour at the temperature range from 300 K to 950 K with the step of 25 K. After such annealing at temperature denoted as T_a the magnetic and electric properties were measured at room temperature.

3. Results

Initial magnetic permeability μ measured at room temperature for samples annealed for one hour at elevated temperatures T_a is shown in Fig. 1. For all examined alloys magnetic permeability passes by a distinct maximum. This fact indicates that application of a suitable one-hour thermal annealing can optimise magnetic properties of these alloys. We define the temperature T_a corresponding

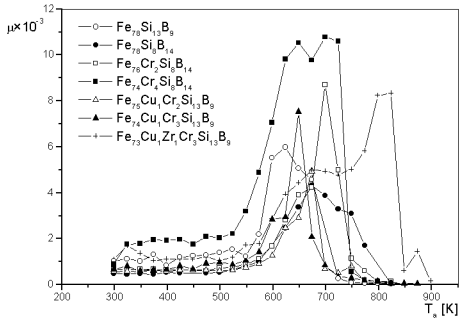

Fig. 1. Initial magnetic permeability μ measured at room temperature for samples after one-hour annealing at temperature T_a.

to the maximum of magnetic permeability $\mu(T_a)$ as the one-hour optimisation temperature — T_{op}.

Figure 2 shows magnetic after-effect $\Delta\mu/\mu$, $\Delta\mu = \mu(t_1) - \mu(t_2)$, where time $t_1 = 30$ s and $t_2 = 1800$ s after demagnetisation and μ at t_1 plotted versus one-hour annealing temperature T_a. As it is known the intensity of magnetic after-effect is directly proportional to concentration of microvoids forming the so-called relaxators [3, 10–17]. In amorphous materials, as a consequence of fast cooling from liquid phase, a relatively high concentration of microvoids is usually observed [9, 10–18]. The diffusion of these defects is mainly responsible for time/thermal instability of amorphous alloys. Obviously such instabilities hinder their practical applications. Magnetic relaxation measurements allow obtaining information about the discussed instabilities and also about the microvoid diffusion.

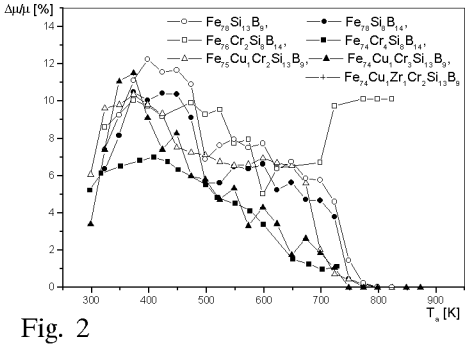

Fig. 2

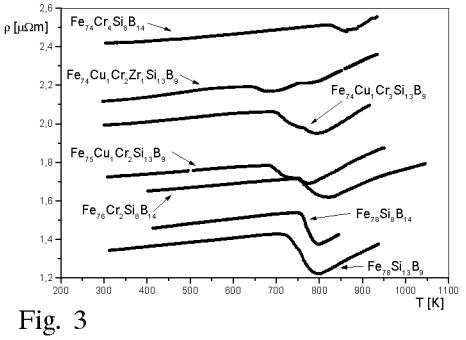

Fig. 3

Fig. 2. Magnetic after-effect $\Delta\mu/\mu$ ($[\mu(t_1) - \mu(t_2)]/\mu(t_1)$, where times $t_1 = 30$ s and $t_2 = 1800$ s after demagnetisation), measured at room temperature for samples after one-hour annealing at temperature T_a.

Fig. 3. Electrical resistivity versus temperature (heating with rate 0.5 K/min).

In amorphous alloys, phase transitions like crystallisation phenomena are usually examined by applying thermal methods, electric and magnetic measurements [19–22]. Figure 3 shows electrical resistivity curves $\rho(T)$ measured by applying linear heating — 0.5 K/min. The drastic decrease in ρ values observed at elevated temperatures is due to crystallisation process. The temperatures of the first and the second stages of crystallisation process were determined from data presented in Fig. 3 by applying the condition $d\rho(T)/dT = 0$.

The characteristic temperatures (i.e. Curie temperatures, one-hour optimisation annealing temperatures and crystallisation temperatures) determined from the data presented in Figs. 1–3 are listed in Table. From this table it can be recognised that the crystallisation temperatures (the first stage — T_1 as well as the second one — T_2) as well as the optimisation temperatures T_{op} are higher than the Curie temperatures. This means that the structural changes responsible

TABLE

Curie temperatures (T_C), one-hour optimisation annealing temperatures (T_{op}) and temperatures of first (T_1) and the second stage (T_2) of crystallisation process.

Material	T_C [K]	T_{op} [K]	T_1 [K]	T_2 [K]
$Fe_{78}Si_8B_{14}$	715	675	730	775
$Fe_{76}Cr_2Si_8B_{14}$	650	675	750	670
$Fe_{74}Cr_4Si_8B_{14}$	645	725	825	845
$Fe_{78}Si_{13}B_9$	650	625	720	750
$Fe_{75}Cu_1Cr_2Si_{13}B_9$	650	675	675	750
$Fe_{74}Cu_1Cr_3Si_{13}B_9$	590	650	685	750
$Fe_{74}Cu_1Cr_2Zr_1Si_{13}B_9$	575	800	635	750

for the optimisation of soft magnetic properties (mainly an increase in magnetic permeability) take place in paramagnetic phase. In such a case the application of room temperature measurements for samples annealed at elevated temperatures is very useful. Typical "*in situ*" measurements obviously are not sufficient [8]. Let us notice that for the base alloys i.e. the $Fe_{78}Si_8B_{14}$ and $Fe_{78}Si_{13}B_9$ we have the reverse relation $T_{op} < T_C$.

4. Discussion and conclusions

The results presented in Fig. 1 (i.e. the dependence $\mu(T_a)$) are to the certain extent typical of amorphous alloys based on iron. In general, magnetic permeability changes in three stages. In the first one, up to the temperature of about $T_{op}-100$ K, μ remains approximately constant. In the second stage at elevated temperatures μ increases rapidly reaching the maximum value at T_{op}. At higher temperatures for $T_a > T_{op}$ a drastic decrease in permeability is observed. All these stages reflect the microstructural changes taking place in examined materials.

The increase in magnetic permeability (even 3–10 times) observed in amorphous alloys, after a suitable thermal annealing (e.g. one-hour annealing at T_{op}) can be explained by different processes: (i) an annealing out of microvoids formed during fast cooling from liquid phase, (ii) a significant decreases in the effective magnetostriction constant and (iii) a formation of a nanocrystalline structure with grain size much smaller than the ferromagnetic exchange length [23, 24]. The detailed analysis of these processes leads to the conclusion that in most cases it is not possible to distinguish between them. The role of a particular process and also its efficiency strongly depend on chemical composition of the examined alloy.

The first mechanism is well demonstrated in Fig. 2, where magnetic after-effect $\Delta\mu/\mu$ is plotted versus T_a. At lower temperatures (up to about 500 K) we observe coagulation and/or a new rearrangements of microvoids which is repre-

sented as a $\Delta\mu/\mu$ maximum. At higher temperatures $\Delta\mu/\mu$ drops down indicating annealing out of migrating defects [13, 14, 16, 17].

Experimental results obtained by X-ray diffraction technique (Fig. 4) and electron microscopy (Fig. 5) observations as well as measurements of magnetic and electric properties show that T_{op} can be both lower and higher than the crystallisation temperature. In the case in which $T_{\mathrm{op}} < T_1$ essentially only two processes — i.e. annealing out of microvoids and decrease in the effective magnetostriction constant — should be taken into account. For $T_{\mathrm{op}} > T_1$ all three processes become important.

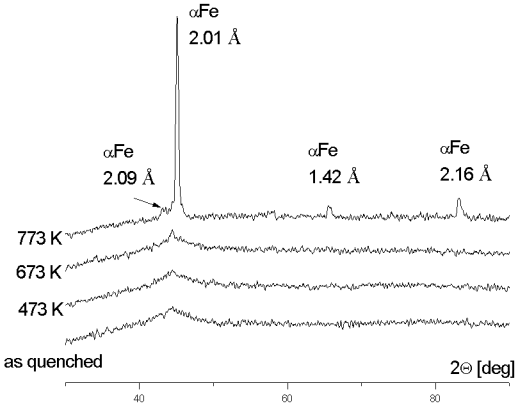

Fig. 4. X-ray diffraction pattern obtained for $Fe_{75}Cu_1Cr_2Si_{13}B_9$ alloy.

Let us consider the first case and assume that $T_{\mathrm{op}} < T_1$. It is known that in amorphous phase magnetic permeability depends on magnetoelastic energy and the so-called stabilisation energy of magnetic domains, which is dependent on microvoid concentration (c). Such approach leads to the following formula for magnetic permeability [2]:

$$\mu(t) \approx \frac{J_{\mathrm{S}}^2 \delta k_{\mathrm{B}} T}{2\mu_0 l\{\frac{3}{2}\lambda_{\mathrm{S}}^{\mathrm{am}}\sigma + pw^2 c[1-\exp(-t/\tau)]\}}, \tag{1}$$

where J_{S}, δ and l are the saturation magnetisation, the effective thickness and domain width, respectively; p is the numerical factor depending on the kind of domain wall, $\lambda_{\mathrm{S}}^{\mathrm{am}}$ is the magnetostriction constant of amorphous phase, σ is the effective stress, w is the interaction energy between spontaneous magnetisation and relaxators (the so-called Néel energy [3]), τ is the relaxation time obeying the Arrhenius relation (for diffusion processes $\tau \propto \exp(E/k_{\mathrm{B}}T)$; E is the activation energy and k_{B} is the Boltzmann constant) and μ_0 is the vacuum magnetic permeability.

In the second case when $T_{\mathrm{op}} > T_1$ the presence of a new nanocrystalline phase should be taken into account [23, 24]. The magnetocrystalline energy K of this phase can be expressed as

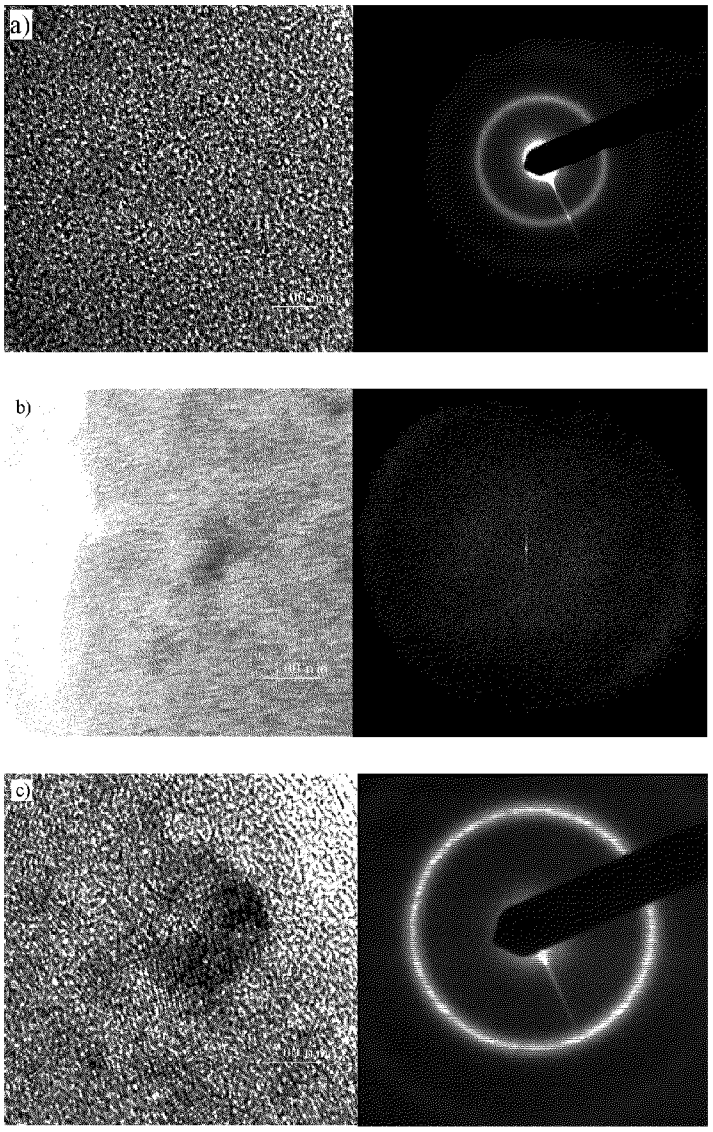

Fig. 5. Electron microscopy image and electro-diffraction pattern obtained after one-hour annealing at optimisation temperature for $Fe_{78}Si_{13}B_9$ (a), $Fe_{75}Cu_1Cr_2Si_{13}B_9$ (b) and $Fe_{75}Cu_1Cr_3Si_{13}B_9$ (c) alloys.

$$K = \left(k_{\mathrm{U}}^2 + \frac{\nu K_1^2 d^3 K^{3/2}}{A^{3/2}} \right)^{1/2}, \tag{2}$$

where ν is the volume fraction of nanocrystalline phase, K_{U} is the induced anisotropy constant of domain structure formed during annealing, d is the mean grain size of the nanocrystalline phase, A is the ferromagnetic exchange energy and K_1 is the anisotropy constant of nanocrystalline phase. For $K_{\mathrm{U}} \ll K_1$ the effective anisotropy

constant can be written as

$$K = \frac{\nu^2 d^6 K_1^4}{A^3} \tag{3}$$

and for $K_U > K_1$ we have

$$K = K_U \left(1 + \frac{\nu K_1^2 d^3}{2A^{3/2}}\right). \tag{4}$$

Assuming the model of random distribution of anisotropy constant of nanocrystalline phase for magnetic permeability one can get the following formula [2, 8]:

$$\mu(t) \approx \frac{12 J_S^2 \delta A^3 k_B T}{24\mu_0 k_B T l\{(K_1^4 d^6 + \frac{3}{2}\lambda_S \sigma A^3) + pw^2 c[1 - \exp(-1/\tau)]\}}, \tag{5}$$

where c is the concentration of microvoids, λ_S is the effective magnetostriction constant, which according to [25] is given by

$$\lambda_S = \nu\lambda_S^C + (1-\nu)(\lambda_S^{am} + k\nu) + \nu\lambda_S^S S/V, \tag{6}$$

where k is the parameter describing the changes of nanostructural phase taking place during crystallisation process; λ_S^C, λ_S^S, are magnetostriction constants for crystalline phase and surface, respectively; the fraction S/V denotes the specific surface of nanocrystals.

Typical value of magnetostriction constant for the $Fe_{78}Si_{13}B_9$ alloy in the "as quenched" state is of about 23×10^{-6} (the magnetostriction constants have been obtained by Villiary method). Thermal annealing causing formation of α-Fe crystallites in amorphous phase reduces this value to 8×10^{-6}, so about 4 times. According to [26] magnetostriction constant of α-Fe crystalline phase is 4×10^{-6}.

Chromium as the alloying addition causes a decrease in effective magnetostriction constant of the alloy and in the same way an increase in magnetic permeability [27, 28]. According to Eq. (5) μ strongly depends on the grain size of nanocrystalline phase. The nanophase formation process is essentially controlled by diffusion phenomena, so strongly depends on temperature and chemical composition of the material. It is known that copper causes an increase in the amount of nucleus of nanocrystalline phase [6]. A relatively high value of inter-surface energy and packing factor can be obtained by adding different alloying additions with large atomic radius. In general, it leads to a slowing down of diffusion processes, so to a decrease in an effective diffusion coefficient.

According to our results the observed increase in magnetic permeability (see Fig. 1) can be attributed to nanocrystallisation process only for two alloys i.e. $Fe_{74}Cu_1Cr_3Si_{13}B_9$ and $Fe_{74}Cu_1Cr_2Zr_1Si_{13}B_9$. For the $Fe_{75}Cu_1Cr_2Si_{13}B_9$ alloy the nanocrystallisation can be excluded because after one-hour annealing at temperature T_{op} the nanocrystalline phase was not detected by applying high resolution electron microscopy (HREM) technique. In contrary to this for the $Fe_{74}Cu_1Cr_3Si_{13}B_9$ alloy one-hour annealing at T_{op} leads to formation of α-Fe(Si) nanocrystalline phase (detected by HREM), though the amount of this phase does

not exceed a few percent. For the $Fe_{74}Cu_1Cr_2Zr_1Si_{13}B_9$ alloy annealing at T_{op} causes formation of the well-developed α-Fe(Si) nanocrystalline phase with grain size of about 20 nm. In this case the optimisation temperature $T_{op} > T_1$.

The main conclusions of the present paper can be summarised as follows:

1. Optimisation of soft magnetic properties in Fe–X–Si–B and Fe–Cu–X–Si–B alloys depends strongly on type and content of alloying additions.
2. The addition of Cr atoms in the Fe–Cr–Si–B alloys improve soft magnetic properties causing a decrease in magnetostriction constant and microvoid contents.
3. Chromium atoms in the $Fe{-}Cu_1{-}Cr{-}Si_{13}{-}B_9$ alloys improve soft magnetic properties, which can be explained in terms of different mechanism i.e. random distribution of anisotropy constant in nanocrystalline phase, changes of magnetoelastic energy and also changes of stabilisation energy of domain structure modified by the presence of microvoids.
4. Copper atoms cause an increase in the amount of nucleus and amount of nanocrystalline phase of small diameter.

Acknowledgments

This work was partially supported by the State Committee for Scientific Research under grant No. 7T08A05317.

References

[1] M.E. Mc Henry, M.A. Willard, D.E. Laughlin, *Prog. Mater. Sci.* **44,** 291 (1999).

[2] J. Rasek, *Some Diffusion Phenomena in Crystalline and Amorphous Metals*, Silesian University Press, Katowice 2000 (in Polish).

[3] G. Haneczok, J. Rasek, *Def. Diff. Forum* **188-190,** 218 (2001).

[4] Z. Stokłosa, P. Kwapuliński, G. Haneczok, J. Rasek, *J. Phys. IV* **8,** 51 (1998).

[5] H. Matyja, T. Kulik, *Trends in Non Crystalline Solids*, Word Sci., Singapore 1992, p. 107.

[6] Y. Yoshizawa, S. Oguma, K. Yamaguchi, *J. Appl. Phys.* **64,** 6044 (1988).

[7] X.Q. Li, X.L. Yang, B.Y. Hu, Z. Wu, Y.Z. Zhang, H.J. Jin, G.Q. Xu, *J. Magn. Magn. Mater.* **145,** 125 (1995).

[8] P. Kwapuliński, J. Rasek, Z. Stokłosa, G. Haneczok, *J. Magn. Magn. Mater.* **234,** 218 (2001).

[9] P. Kwapuliński, J. Rasek, Z. Stokłosa, G. Haneczok, M. Gigla, *J. Magn. Magn. Mater.* **215-216,** 334 (2000).

[10] R. Grössinger, R. Sato-Turtelli, *IEEE Trans. Magn.* **30,** 455 (1994).

[11] P. Allia, F. Vinai, *Phys. Rev. B* **26,** 6141 (1982).

[12] P. Allia, F. Vinai, *Phys. Rev. B* **33,** 422 (1986).

[13] H. Kronmüller, *Philos. Mag. B* **48,** 2 (1983).

[14] B. Zegrodnik, G. Haneczok, J. Rasek, *Mater. Sci. Arch.* **15,** 161 (1994).

[15] Z. Stokłosa, P. Kwapuliński, J. Rasek, J. Ilczuk, J. Lelątko, *Acta Phys. Pol. A* **89,** 437 (1996).

[16] F. Rettenmeier, H. Kronmüller, *Phys. Status Solidi A* **93,** 221 (1986).

[17] F. Rettenmeier, E. Kishi-Koszo, H. Kronmüller, *Phys. Status Solidi A* **93,** 597 (1986).

[18] A. Van den Beukel, E. Huizer, *Scr. Metall.* **19,** 1327 (1985).

[19] K. Pękala, P. Jaśkiewicz, T. Kulik, *Nanostructured Mater.* **4,** 707 (1994).

[20] A. Inoue, *Bulk Amorphous Alloys*, Trans. Tech. Publications, Switzerland 1998.

[21] M. Barandiaran, L.F. Barquin, J.C.G. Sal, P. Goria, A. Hernando, *Solid State Commun.* **88,** 75 (1993).

[22] G. Rontino, G.W. Koebruge, M. Baricco, J. Sietsma, *Phys. Status Solidi B* **179,** 315 (1993).

[23] G. Herzer, *J. Magn. Magn. Mater.* **157-158,** 133 (1996).

[24] G. Herzer, L.L. Varga, *J. Magn. Magn. Mater.* **215-216,** 506 (2000).

[25] A. Ślawska-Waniewska, *J. Phys. IV* **8,** 11 (1998).

[26] R. M. Bozorth, *Ferromagnetism*, IEEE Press, New York 1993.

[27] M.N. Chandrasekhariach, *Metalic Glasses*, Trans. Tech. Publications, Switzerland 1984, p. 269.

[28] Z. Kaczkowski, in: *Amorphous Metallic Materials*, Ed. H.K. Lachowicz, Institute of Physics PAN, Warsaw 1983, p. 68.